

Continuum Model of Gas Uptake for Inhomogeneous Fluids

Yungok Ihm,^{*,†,‡,§} Valentino R. Cooper,[§] Lukas Vlcek,[§] Pieremanuele Canepa,^{||,⊥}
Timo Thonhauser,^{||,#} Ji Hoon Shim,[†] and James R. Morris^{§,‡}[†]Department of Chemistry, Pohang University of Science and Technology, Pohang 790-784, Korea[‡]Department of Materials Science and Engineering, University of Tennessee, Knoxville, Tennessee 37996, United States[§]Materials Science and Technology Division, Oak Ridge National Laboratory, Oak Ridge, Tennessee 37831, United States^{||}Department of Physics, Wake Forest University, Winston-Salem, North Carolina 27109, United States[⊥]Materials Science Division, Lawrence Berkeley National Laboratory, Berkeley, California 94720, United States[#]Department of Chemistry, Massachusetts Institute of Technology, Cambridge, Massachusetts 02139, United States

S Supporting Information

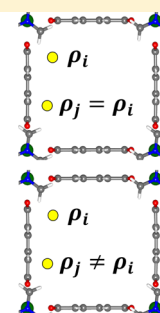
ABSTRACT: We describe a continuum model of gas uptake for inhomogeneous fluids (CMGIF) and use it to predict fluid adsorption in porous materials directly from gas-substrate interaction energies determined by *first-principles* calculations or accurate effective force fields. The method uses a perturbation approach to correct bulk fluid interactions for local inhomogeneities caused by gas-substrate interactions, and predicts local pressure and density of the adsorbed gas. The accuracy and limitations of the model are tested by comparison with the results of grand canonical Monte Carlo simulations of hydrogen uptake in metal-organic frameworks (MOFs). We show that the approach provides accurate predictions at room temperature and at low temperatures for less strongly interacting materials. The speed of the CMGIF method makes it a promising candidate for high-throughput materials discovery in connection with existing databases of nanoporous materials.

Homogeneous fluid

$$E_i$$
$$\downarrow \rho_i - P_i - T$$
$$\rho_i$$

Inhomogeneous fluid

$$\delta\varphi \sim (\rho_j - \rho_i)E_{ij}(r_{ij})$$
$$\delta\rho(r_i) \sim -\rho_i^0 \delta\varphi(r_i)/k_B T$$



1. INTRODUCTION

Gas storage and separation is one of the most pressing research issues for solving energy and environmental problems worldwide. Over the past decades, computation has made great contributions to the development of efficient materials and technologies for energy storage and flue-gas separation.^{1–3} In the design and development of promising materials for renewable energy generation and greenhouse gas capture lies the search of porous media with high surface area and pore volume that are directly associated with high gas uptake capacities.⁴ For the calculation of the gas uptake in porous materials, the grand canonical Monte Carlo (GCMC) method is routinely used.^{2,5,6} We recently proposed a continuum model (CM) that calculates the gas uptake capacities directly from gas-substrate interaction energies.^{7–11} The method uses the gas-substrate interaction energy to obtain the chemical potential and the pressure of the adsorbed gas, which can then be converted to the density using the equation of state (EOS) of the homogeneous bulk gas. The method can successfully predict the hydrogen and methane uptake capacities on model slit pores and real microporous carbon materials.^{7,8}

Despite the success of our model in gas uptake calculations on microporous carbons, its applicability may be limited at low temperatures for highly confined systems with strongly inhomogeneous gas-substrate interactions, such as MOFs.

The main reason lies in large deviations from ideality, resulting in the need to account more accurately for close packing effects and overall atom-atom correlations at the atomic scale.

Here, we propose an integrated approach targeting the prediction of the gas uptake capacities of porous media with stronger inhomogeneity in gas-substrate interactions. The methodology starts with the initial estimation of adsorption density distributions based on bulk gas EOS and known fluid-substrate interaction potential, as described in refs 7 and 8. The atomistic gas-gas correlations in the inhomogeneous environment are then taken into account as a perturbation to the gas interactions in bulk fluid. The calculated density change due to the perturbation is consequently used to adjust the adsorption density throughout the pore volume. The method was tested with hydrogen storage on a prototypical MOF, Zn(BDC)-(TED)_{0.5},¹² at both room and liquid nitrogen temperatures. This prototypical MOF exhibits strong repulsive and attractive interactions with H₂ fluid resulting in high and strongly anisotropic adsorption densities. We find that the proposed method successfully predicts overall hydrogen uptake as well as local densities except within the vicinity of some strongly interacting surface sites. For systems with highly attractive sites

Received: May 18, 2017

Revised: July 19, 2017

Published: July 20, 2017

at low temperatures, development of a more complete, nonperturbative theoretical treatment would be needed. Within this limitation, the method provides a rapid, reasonably accurate approach to predicting uptakes even for systems in which the adsorbent medium has highly variable adsorption strengths.

2. CONTINUUM MODEL OF GAS UPTAKE FOR INHOMOGENEOUS FLUIDS (CMGIF)

In this section, we briefly review our prior approach to directly calculating uptakes, and the limitations that arise due to its local nature. We then present a refinement of this approach that incorporates corrections for nonlocal behavior within the fluid.

2.1. Continuum Model (CM) of Gas Uptake for Homogeneous Fluids. Our original thermodynamic model calculates the gas storage directly from the gas-substrate interaction energies and bulk gas EOS.^{7,8} The model starts by assuming that the adsorbed local gas is in thermodynamic adsorption/desorption equilibrium with the external gas and thus their chemical potentials are equal. Also, as the local gas interaction is comprised of gas-gas and gas-solid interactions, the local adsorption/desorption equilibrium is described by the following relation:

$$\mu_{\text{ext}} = \mu_i = \mu_i^{\text{g}} + E_i \quad (1)$$

where μ_{ext} and μ_i are the chemical potential of the external and local gas, respectively. μ_i^{g} and E_i are the components of the local gas chemical potential that account for the gas-gas and gas-solid interactions, respectively. The μ_i^{g} , which shall be called “gas-component chemical potential” is expressed in terms of the fugacity.

$$\mu_i^{\text{g}} = \mu_{\text{ext}} + k_{\text{B}}T \ln(f_i/f_{\text{ext}}) \quad (2)$$

Here, the fugacity f is a fictitious pressure which bridges the chemical potential to thermodynamics variables of real gases, and is related to the real gas pressure by the fugacity coefficient, $\Psi = f/P$. For ideal gases, the fugacity equals to the pressure. Once the fugacity of the local gas is obtained by using eqs 1 and 2, the local gas pressure can readily be obtained from the gas-substrate interaction energies alone.

$$P_i = (\Psi_{\text{ext}}/\Psi_i)P_{\text{ext}} \exp(-E_i/k_{\text{B}}T) \quad (3)$$

Here P_{ext} , P_i and Ψ_{ext} , Ψ_i are the pressures and the fugacity coefficients of the external gas and those of the adsorbed local gas at grid site i , respectively. The E_i and k_{B} are the fluid-solid interaction energy and Boltzmann constant. Once the local pressure is obtained, the local gas density is estimated with the bulk gas EOS:

$$f(P, \rho, T) = 0 \quad (4)$$

In the present work, the data from Linstrom and Mallard¹³ (available at <http://webbook.nist.gov/chemistry/fluid/>) that uses the EOS proposed by Leachman et al.¹⁴ are used to obtain H_2 density from its pressure. See Figure S1 for EOS data of H_2 used in this work. The total uptake N is then calculated using

$$N(P) = \sum_i \rho_i(P) dV_i \quad (5)$$

where $\rho_i(P)$ and dV_i are the density at pressure P and the pore volume of the grid site i , respectively.

The CM described above deals with the local properties assuming that the entire fluid system is uniform, i.e., $\rho = \rho_i$ everywhere. This approach may reasonably approximate the

near homogeneous densities that occur in, e.g., microporous carbons. When the fluid-solid interactions become highly inhomogeneous, however, this approach starts to break down because the densities at each site (ρ_i) obtained with CM now deviate significantly from the density at the site of interest, ρ_i . The deviations in densities, $\rho_j - \rho_i$, need to be taken into account in terms of deviations in fluid-fluid interactions, which are then treated as perturbations in our proposed scheme. The perturbations now give rise to changes in local densities and final gas storage capacities as described in the following section.

2.2. Inhomogeneous Fluid-Fluid Interactions: Perturbation to the Homogeneous Fluid. CMGIF starts with the CM described above to calculate the initial local gas densities ρ_i^0 under the assumption that the fluid densities are uniform and the fluid-fluid interactions are homogeneous. However, interactions in inhomogeneous fluids can deviate significantly from those in bulk. Such differences can be taken into account as a perturbation with homogeneous bulk fluid as a reference. For practical applications we will map the pore volume onto a grid, which, in principle, may be nonuniform, with grid points i associated with volume ΔV_i . The gas-substrate interaction energies are calculated at all grid sites and the gas sorption densities at the corresponding grid volumes are computed with CMGIF. The first approximation to the densities may be calculated using eqs 1–4 to determine a local density ρ_i^0 at all sites i . However, nonlocal fluid-fluid interactions with atoms near site i will result in deviations from the local approximation. The perturbation, which is this deviation in fluid-fluid interaction energies per particle may be written as

$$\delta\varphi(\mathbf{r}_i) = \sum_j \Delta V_j (\rho_j^0 - \rho_i^0) E_{ij}(\mathbf{r}_{ij}) \quad (6)$$

because the interaction energy between i and j with densities ρ_i^0 and ρ_j^0 is $(\rho_i^0 \Delta V_i)(\rho_j^0 \Delta V_j) E_{ij}$, with E_{ij} being the effective fluid-fluid interaction energy defined in subsection 3.1.2. A system with uniform fluid density ρ^0 exposed to weak external perturbation $\delta\varphi$ undergoes the change in density as follows:¹⁵

$$\delta\rho(\mathbf{r}_i) = -\rho_i^0 \delta\varphi(\mathbf{r}_i)/k_{\text{B}}T - (\rho_i^0)^2/k_{\text{B}}T \sum_j h(\mathbf{r}_i - \mathbf{r}_j) \delta\varphi(\mathbf{r}_j) \quad (7)$$

where $h(\mathbf{r}_i - \mathbf{r}_j)$ is the total pair-correlation function of the interacting fluid as described in eq 10 for H_2 . This relation, known as the Yvon equation,¹⁵ is equivalent to the Taylor expansion of ρ with respect to $\delta\varphi$. We use this expression together with eq 6 to calculate the density change in inhomogeneous fluids compared to the uniform fluids. The density change combined with the initial density obtained using the CM gives the net local fluid density.

3. HYDROGEN STORAGE IN $\text{Zn}(\text{BDC})(\text{TED})_{0.5}$ AND Mg-MOF-74 USING CMGIF

3.1. Methods. As a specific application of the proposed formalism, we examine H_2 storage in MOF structures with the goal of accurately predicting uptake at finite temperatures and pressures. The calculations are compared with grand canonical Monte Carlo simulations, based on empirical H_2 - H_2 interactions. We consider parametrizations based on both our *first-principles calculations* and previously established empirical H_2 -MOF interactions.

3.1.1. MOF Structures and H₂–MOF Interactions. The experimental structures of Zn(BDC)(TED)_{0.5}¹² (BDC: 1,4-benzene-amide; TED: triethylenediamine) (Figure 1A) and

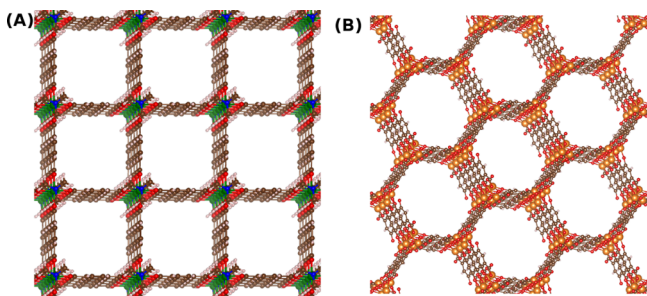


Figure 1. (A) Structure of Zn(BDC)(TED)_{0.5} and (B) structure of Mg-MOF-74.

Mg-MOF-74¹⁶ (Mg₂(DOT); DOT = 2,5-dioxidoterephthalate) (Figure 1B) were taken. Zn(BDC)(TED)_{0.5} has a tetragonal structure with $a = b = 10.93$ Å and $c = 9.61$ Å; Mg-MOF-74 has a hexagonal structure with $a = 25.88$ Å and $c = 6.88$ Å.

The binding energy of H₂ is also calculated using the van der Waals density functional (vdW-DF),¹⁷ as implemented in Quantum ESPRESSO.¹⁸ To correctly capture the weak van der Waals (vdW) forces—which are critical in this study—we use the nonlocal vdW-DF,¹⁷ which uses revPBE for exchange.^{17,19–21} Ultrasoft pseudopotentials (with the following electronic configurations C 2s² 2p², O 2s² 2p⁴, H 1s, Mg 2p⁶ 3s² and Zn 3d¹⁰ 4s²) in combination with wave function and density cutoffs of 480 and 4800 eV were used, and the energy was sampled at the Γ point. The total energy convergence was set to 10^{−7} eV, and total forces were relaxed to less than 0.01 eV/Å.

To assess the accuracy of the CMGIF approach, we generated reference data using GCMC simulations. In these classical simulations, H₂–H₂ interactions were represented by the Buch potential.²² In the first set of simulations, H₂–MOF interactions were represented by the universal force field (UFF) of Rappe et al.²³ using the Lorentz–Berthelot combining rule. In the second set of simulations, the H₂–MOF interactions were described directly using the vdW-DF energies. At 77 K, the quantum effects were incorporated into the H₂–MOF interaction using the quadratic Feynman–Hibbs formalism in eq 8,²⁴

$$U_{\text{H}_2\text{-MOF}}^{\text{FH}}(\mathbf{r}) = U_{\text{H}_2\text{-MOF}}(\mathbf{r}) + \frac{\hbar^2}{24\mu k_{\text{B}}T} \nabla^2 U_{\text{H}_2\text{-MOF}}(\mathbf{r}) \quad (8)$$

where μ is the reduced mass of H₂–MOF interaction, which is the mass of the H₂ molecule. $U_{\text{H}_2\text{-MOF}}$ is the H₂–MOF interaction energy calculated using either UFF or vdW-DF. The GCMC simulations were equilibrated over 2×10^5 individual MC steps and the production runs comprised 10^7 individual MC steps. The MC moves included random translational and insertion–deletion moves with the relative probability of each set to 0.5, and the acceptance rate for the translational moves set to 0.5. The simulations were performed with an in-house code.

3.1.2. The Pair-Potential and -Correlation Function for H₂–H₂ Interaction. We divide the region for the fluid–fluid interaction ($E_{ij}(r)$ in eq 6) into two separate areas: (1) local ($r \leq r_0$) and (2) nonlocal ($r > r_0$), with r_0 being the distance at

which the pair-distribution function starts to become zero. The pair-distribution function is defined as $g(r) = h(r) + 1$ associated with $h(r)$ defined in eq 10 for H₂. At $r < r_0$, the pair-distribution function is zero and any two particles are not to be located within r_0 in distance due to strong particle–particle repulsion. The nonlocal region accounts for the pairwise interaction of the test H₂ located at i with the surrounding H₂ molecules and it ranges from r_0 to infinity. The interaction between the test H₂ and the surrounding H₂ in this region is described by the Lennard–Jones potential with Buch’s parameters, which is truncated at 10 Å.²² For the local region where the H₂–H₂ pair-distribution function is zero, a constant repulsive potential is assigned, for reasons described below, giving the final potential between two sites i and j as follows:

$$\begin{aligned} E_{ij}(r_{ij})/k_{\text{B}} &= C(r_{ij} \leq r_0) \\ &= 4\epsilon \left(\left(\frac{\sigma}{r_{ij}} \right)^{12} - \left(\frac{\sigma}{r_{ij}} \right)^6 \right) (r_0 < r_{ij} \leq r_c) \\ &= 0(r_{ij} > r_c) \end{aligned} \quad (9)$$

with $\epsilon = 34.2$ K, $\sigma = 2.96$ Å, $C = 250$ K, $r_0 = 2.66$ Å, and $r_c = 10$ Å. The ϵ and σ are from ref 22 and r_c is the cutoff distance beyond which the gas uptake capacities stay nearly constant. The r_0 is the separation distance where $h(r)$ in eq 10 becomes zero and is chosen so that both the pair-potential and the pair-correlation function are repulsive at $r < r_0$.

The reason for assigning a constant repulsive potential for the local potential is the following—the perturbation $\delta\varphi(r_i)$ may be obtained by calculating the difference in chemical potential change for introducing a single test particle to i in inhomogeneous and homogeneous fluids and the local and nonlocal regions affect the final perturbation differently. The nonlocal region contributes to the chemical potential change of the test H₂ by changing the interactions between the test H₂ and surrounding H₂ molecule—the density maps of the surrounding H₂ molecules are different in the homogeneous and inhomogeneous fluids. In contrast, the local region ($r \leq r_0$) contributes to the chemical potential change of the test H₂ by changing the affinity of H₂ to i : the affinity of the test H₂ to a site with stronger H₂–MOF interaction should be larger than that to a less strongly interacting sites. Because introducing two particles simultaneously to sites within r_0 in distance is forbidden (pair-distribution function is zero), high affinity of H₂ to a neighboring site (within r_0 from i) decreases effective affinity of a test H₂ to i , resulting in increase of the effective chemical potential change associated with the introduction of a test H₂ to i . This effect may be modeled with a constant, repulsive potential between i and neighboring sites within r_0 as shown with C in eq 9. The constant and repulsive local potential is then chosen as an adjustable free parameter specific for fluid systems, which is H₂ in this case. Our calculations show that a constant repulsive local potential of $C = 250$ K works well for describing the H₂ uptake in Zn(BDC)(TED)_{0.5}. The pair-correlation function used in this work was obtained by fitting the functional form in eq 10 to the H₂ pair-correlation data at 17 K from Celli et al.²⁵ (Figure S2).

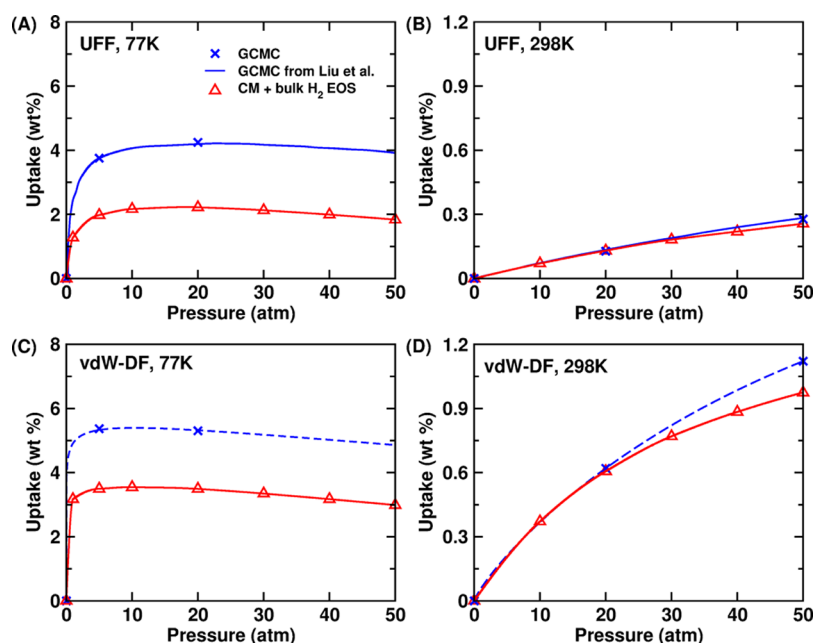


Figure 2. Comparison between the H_2 uptake capacities of GCMC and CM for $\text{Zn}(\text{BDC})(\text{TED})_{0.5}$. Blue crosses, our GCMC results; blue solid line, GCMC results from Liu et al.;⁵ red triangle, CM results; blue dotted line, fitting of our GCMC results for vdW-DF. (A) UFF at 77 K. (B) UFF at 298 K. (C) vdW-DF at 77 K. (D) vdW-DF at 298 K.

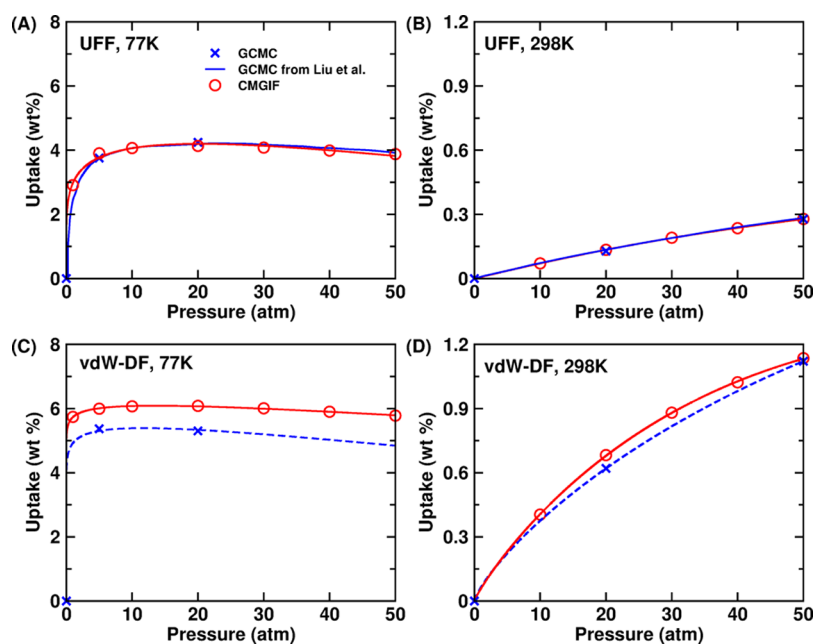


Figure 3. Comparison between the H_2 uptake capacities of GCMC and CMGIF for $\text{Zn}(\text{BDC})(\text{TED})_{0.5}$. Blue crosses, our GCMC results; blue solid line, GCMC results from Liu et al.;⁵ red circle, CMGIF results; blue dotted line, fitting of our GCMC results for vdW-DF. (A) UFF at 77 K. (B) UFF at 298 K. (C) vdW-DF at 77 K. (D) vdW-DF at 298 K.

$$h(r) = (A_0/r) \exp\left(\frac{-r}{r_1}\right) \sin(r/r_2) (r \geq r_0)$$

$$= -1 \quad (\text{otherwise}) \quad (10)$$

with $A_0 = 9.437 \text{ \AA}$, $r_1 = 2.923 \text{ \AA}$, and $r_2 = 0.48 \text{ \AA}$.

3.1.3. H_2 Uptake Calculations. The hydrogen uptake capacities of both MOFs were calculated using the CM and CMGIF method at 298 and 77 K. At 77 K, Feynman-Hibbs effective potential in eq 8 was used to incorporate quantum effects at low temperature. The computed uptakes follow the

definition of Liu et al.⁵ with the pore volume of $0.73 \text{ cm}^3/\text{g}^5$ for $\text{Zn}(\text{BDC})(\text{TED})_{0.5}$ and $0.63 \text{ cm}^3/\text{g}^{26}$ for Mg-MOF-74, respectively.

3.2. Results and Discussion. **3.2.1. Hydrogen Storage Capacity of $\text{Zn}(\text{BDC})(\text{TED})_{0.5}$ from CM.** The performance of CM and CMGIF was evaluated for comparison with the H_2 uptake on a prototypical MOF, $\text{Zn}(\text{BDC})(\text{TED})_{0.5}$ at 298 and 77 K. $\text{Zn}(\text{BDC})(\text{TED})_{0.5}$ is a highly porous and hydrophobic MOF with tetragonal structure (Figure 1A).¹² The measured Brunauer–Emmett–Teller (BET) surface area and pore volume of this MOF are $1794 \text{ m}^2/\text{g}$ and $0.65 \text{ cm}^3/\text{g}$,

respectively. $\text{Zn}(\text{BDC})(\text{TED})_{0.5}$ has two different channels of sizes $7.5 \text{ \AA} \times 7.5 \text{ \AA}$ (channel A) and $4.8 \text{ \AA} \times 3.2 \text{ \AA}$ (channel B), respectively.^{27,28} Strong H_2 binding sites are located inside these two channels but are not specifically associated with the reactivity of the Zn sites, whose electrons are completely used to bond the MOF linkers and thus not available for binding gas molecules in the MOF pore. Our vdW-DF calculation gives $\sim -10 \text{ kJ/mol}$ interaction energy at the strongest H_2 binding site in channel B, while UFF gives $\sim -5.7 \text{ kJ/mol}$ at the same site. The H_2 -MOF interaction energies calculated with the UFF and vdW-DF were first used to calculate the hydrogen densities and the excess uptake capacities at 77 and 298 K using the CM. The quantum effects are included at 77 K through the Feynman-Hibbs effective potential.

Figure 2 compares the H_2 uptake capacities of $\text{Zn}(\text{BDC})(\text{TED})_{0.5}$ calculated by GCMC (blue) and CM (red) at 298 and 77 K. The H_2 -MOF interaction energies were calculated with UFF (Figure 2A and B) and vdW-DF (Figure 2C and D). As UFF gives H_2 -MOF interaction energies that are about half of those of vdW-DF, the calculated uptakes for the UFF are much lower than those of vdW-DF. The results show that the CM at room temperature gives consistent results with those of GCMC for both the UFF and vdW-DF (Figure 2B and D). At room temperature, the calculated H_2 densities at the strongest binding site in channel B are 14 and 32 mol/L for the UFF and vdW-DF, respectively. At 77 K, however, the CM significantly underestimates capacities compared to GCMC (Figure 2A and B). At 77 K and 20 atm, the H_2 uptake capacities of $\text{Zn}(\text{BDC})(\text{TED})_{0.5}$ calculated by CM are only 52% and 66% of those by GCMC, for UFF and vdW-DF, respectively, indicating the limitation of using the bulk gas EOS in CM. However, although the densities, particularly at the strong binding sites, might have been underestimated, the H_2 densities at the strongest binding site in channel B are 50 and 65 mol/L for the UFF and vdW-DF, respectively, which are already fairly large.

3.2.2. Hydrogen Storage Capacity of $\text{Zn}(\text{BDC})(\text{TED})_{0.5}$ with CMGIF. The H_2 storage capacities of $\text{Zn}(\text{BDC})(\text{TED})_{0.5}$ were calculated with CMGIF using the results obtained in subsection 3.2.1 as initial H_2 densities for the calculations of the perturbation and density correction. While the average density inside the pore increases negligibly at room temperature, there are appreciable bulk density increases inside the pore at 77 K: 74% and 0.5% increase for UFF and 68% and 13% increase in average density using CMGIF at 77 and 298 K, respectively. The reason an inhomogeneous model is necessary is that, at the lower temperatures, sites with the same adsorption strength have different densities, due to interactions with the fluids in the surrounding regions. These density changes are incorporated into the calculations of the H_2 uptake capacities. Figure 3 depicts the CMGIF calculated capacities of H_2 uptake for both the UFF and vdW-DF at 77 and 298 K. One can see that CMGIF increases the H_2 uptake capacities significantly compared to those with CM, and now the isotherms calculated by CMGIF show excellent agreement with those of GCMC for the UFF at both 77 K (Figure 3A) and 298 K (Figure 3B) and for the vdW-DF at 298 K (Figure 3D). For vdW-DF at 77 K, the CMGIF gives an overestimation of less than 15% compared to GCMC (Figure 3C). The errors computed with vdW-DF at 77 K originate from the increased ρ^0 and $\delta\varphi$ obtained at low temperatures due to strong H_2 -MOF interactions compared to UFF.

Figure 4 shows the initial and corrected densities of hydrogen at the strongest binding site located at channel B.

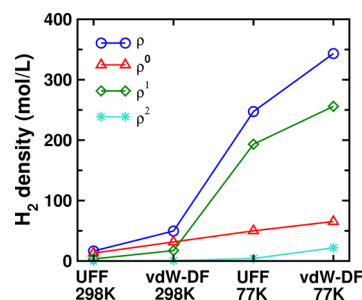


Figure 4. H_2 uptake densities at the strongest binding site in channel B. Blue circle, final density by CMGIF; red triangle, initial density by CM; green diamond, density change by the first term of the Yvon equation; cyan star, density change by the second term of the Yvon equation.

The data are taken for the external pressures of 20 and 50 atm, for 77 and 298 K, respectively. CMGIF gives density corrections of less than 50% at 298 K for both the UFF and vdW-DF. In contrast, the density corrections at 77 K are noticeable. For the UFF, with the initial H_2 density of 50 mol/L, CMGIF predicts the final density of 250 mol/L at the strongest binding site in channel B. Given that the maximum bulk H_2 density at 77 K is less than 100 mol/L, this density is quite remarkable, illustrating that strong MOF- H_2 interactions achieve a packing far beyond the maximum bulk H_2 packing limit. It is also evident that ρ^1 (the first term of Yvon equation), which is dominant over ρ^2 (the second term) increases with the increasing initial density ρ^0 . For example, the initial density ρ^0 are 13 and 32 mol/L for the UFF and vdW-DF, respectively. Their ρ^1 are 3 and 17 mol/L. At 77 K, the initial density ρ^0 are 51 and 66 mol/L for the UFF and vdW-DF, respectively, and their ρ^1 are 192 and 256 mol/L. This shows that the density correction would keep increasing with the increased initial fluid density and at some large fluid density, the proposed perturbative density correction scheme would start to break down. It appears that vdW-DF at 77 K could fall into that regime. For such cases, a more thorough density correction scheme would be desirable for accurate prediction of gas storage for general conditions.

3.2.3. Effects of the Repulsive Local Potential. The perturbation energy $\delta\varphi$ sensitively depends on the accuracy of the pair-potential $E_{ij}(r_{ij})$. The nonlocal ($r_{ij} > r_0$), interparticle interactions are taken from Buch et al.,²² which has been successfully used in many works.^{5,29} In this section, we demonstrate how sensitively the accuracy of the CMGIF depends on the strength of the constant repulsive local potential (C in eq 9). The initial H_2 density solely originates from the H_2 -MOF interactions and bulk H_2 EOS. As ρ^1 dominates over ρ^2 , the density correction by ρ^1 will mainly be considered for the discussions. The density correction ρ^1 takes place in pairwise manner, i.e., $\rho_i^1 \sim \rho_i^0 (\rho_i^0 - \rho_j^0) E_{ij}(r_{ij})$ and $\rho_j^1 \sim \rho_j^0 (\rho_j^0 - \rho_i^0) E_{ij}(r_{ij})$. As $E_{ij}(r_{ij}) = E_{ji}(r_{ji})$, the net density correction via pairwise interaction involving site i and j , which is $\rho_i^1 + \rho_j^1 \sim (\rho_i^0 - \rho_j^0)^2 E_{ij}(r_{ij})$, increases with increasing $E_{ij}(r_{ij})$. Note that $E_{ij}(r_{ij})$ has two parts: (1) nonlocal Lennard-Jones potential and (2) local, constant repulsive potential, as described in eq 9. Our initial calculations using the CM underestimated the H_2 uptake capacities compared to GCMC. To increase the net H_2 density, the density correction via pairwise interaction needs to be positive, which illustrates the importance of the reasonably strong repulsive local potential. We find that the accuracy of CMGIF sensitively depends on the choice of this repulsive local

potential (Figure 5). For example, increasing the repulsion from $C = 250$ to 300 K increases the uptake from 4 to 5.3 wt %

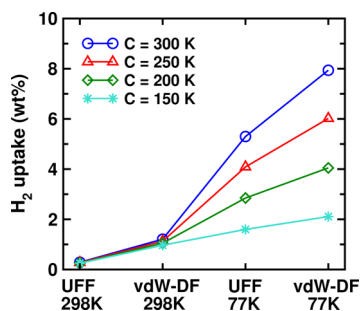


Figure 5. Effect of the strength of the repulsive local potential in eq 9 on H_2 uptake capacity.

at 77 K and 20 atm for UFF. Under the same conditions, CMGIF increases the uptake from 6 to 8 wt % for vdW-DF. We also find that a repulsive potential strength of $C = 250$ K, which is ~ 10 times larger than the Lennard–Jones potential well gives the results most consistent with GCMC. The excellent performance achieved with CMGIF using a single adjustable parameter is surprising because our prior efforts suggest that it is extremely difficult to find a method providing accurate density corrections to our CM model, with one or two adjustable parameters, at both the room and low temperatures. Ideally, one would determine the parameter C with a set of materials providing varying degree of inhomogeneous fluid–solid interactions (training set), and more rigorous evaluation on the performance of CMGIF may be conducted with a test set of materials. Although legitimate predictive power of CMGIF should be achieved after those thorough trainings and evaluations, the purpose of the current paper is rather focused on demonstration of the methodology rather than evaluations.

3.2.4. H_2 Uptake in Mg-MOF-74. Mg-MOF-74 has a slightly skewed hexagonal honeycomb structure with a diameter of ~ 11

Å (Figure 1B).¹⁶ Unlike Zn(BDC)(TED)_{0.5}, Mg-MOF-74 has coordinatively unsaturated open metal sites and thus provides strong H_2 binding sites specifically associated with these open metals.^{30,31} To map the potential energy surface (PES) of the MOF we built more than 200 configurations of H_2 molecules interacting with the MOF structure, utilizing a dense mesh spanning the entire MOF channel. In practice, one of the H atoms of the H_2 molecule was placed at each point of the mesh. To produce a coherent PES, the coordinates of the MOF scaffold were kept fixed during the relaxation, while the H_2 coordinates were optimized. Using this construction in combination with the vdW-DF functional, the strongest binding energy was ~ 0.126 eV. This value is slightly more positive than what was previously reported by relaxing the entire MOF structure and H_2 positions (~ 0.16 eV)³⁰ but substantially more accurate than the binding energy evaluated by UFF that gives only ~ 0.065 eV.

Figure 6 depicts the comparison of the calculated H_2 uptakes of Mg-MOF-74 by the original CM and newly developed CMGIF. As expected, CMGIF gives only minor increase in uptakes compared to using CM at room temperature (Figure 6B and D). At 77 K, however, there are noticeable increases in uptakes for both the UFF and vdW-DF (Figure 6A and C). We also notice that the saturation of the uptake occurs at lower pressures as the H_2 –MOF interaction energies and the uptakes increase. Whereas the saturation pressure is much higher than 50 atm at room temperature for both the UFF and vdW-DF, CMGIF calculated maximum H_2 uptake of 1.7 wt % occurs at 10 atm for UFF at 77 K. The saturation of the excess uptake occurs at even lower pressure of < 1 atm for the vdW-DF at 77 K and it is associated with the fact that the increased inhomogeneity in densities in Mg-MOF-74 calculated by CMGIF at low temperature drives early saturation of the uptake in this system. It should be noted here that although vdW-DF (with the revPBE exchange) systematically overestimates van der Waals separation distances, it provides

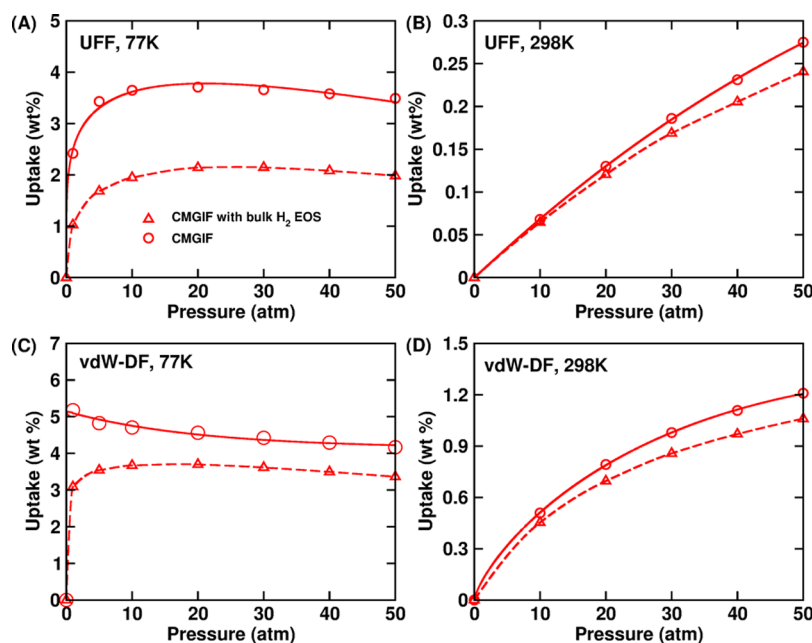


Figure 6. H_2 uptake capacities of Mg-MOF-74. Red triangle, CM results; red circle, CMGIF results. (A) UFF at 77 K. (B) UFF at 298 K. (C) vdW-DF at 77 K. (D) vdW-DF at 298 K.

excellent values for the interaction energies, and thus may be more suitable for this approach.

4. CONCLUSIONS

We have developed a perturbative model of gas uptake (CMGIF), which is designed to deal with the inhomogeneities arising from gas–substrate interactions. The method initially calculates the gas adsorption densities with a continuum model that uses the gas–pore interactions and the bulk fluid Equation of State. The fluid densities are then corrected by incorporating the inhomogeneous fluid–fluid interactions into a perturbation energy that leads to density changes. We find that the correction in densities and uptakes is strongly controlled by the accuracy of the pair-potential, and the repulsive local potential, in particular. Although true predictive power of CMGIF may be achieved with a more rigorous parametrization on a training set encompassing varying degree of inhomogeneous gas–substrate interactions, our results demonstrate that CMGIF gives results consistent with the grand canonical Monte Carlo method at enormously fast speed. It takes only ~2 min on an Intel Xeon E5 processor to calculate H₂ uptake of Zn(BDC)(TED)_{0.5} at a given pressure. Our work with the CM and CMGIF shows that the effect of inhomogeneous adsorbate–adsorbent interactions on the inhomogeneity of the fluid densities is prominent at low temperatures, while it is only minor at room temperature. However, given that CMGIF is computationally inexpensive, it would be desirable to assume that the fluid densities of the systems and the conditions under study are inhomogeneous and compute the gas storage capacity using both the CM and CMGIF and decide whether the fluid behavior deviates from those of bulk fluids. With the accuracy comparable to GCMC and outperformance in terms of speed, CMGIF offers a promising opportunity for sorption-based high-throughput materials discovery for a broad class of porous materials and conditions.

■ ASSOCIATED CONTENT

Supporting Information

The Supporting Information is available free of charge on the ACS Publications website at DOI: 10.1021/acs.jpcc.7b04834.

Equation of state of molecular hydrogen at 77 and 298 K; total pair-correlation function of molecular hydrogen (PDF)

■ AUTHOR INFORMATION

Corresponding Author

*E-mail: yungokihm@postech.ac.kr.

ORCID

Yungok Ihm: 0000-0002-8070-0757

Lukas Vlcek: 0000-0003-4782-7702

Pieremanuele Canepa: 0000-0002-5168-9253

Notes

The authors declare no competing financial interest.

■ ACKNOWLEDGMENTS

Y.I. and J.H.S. were supported by the Global Frontier Program through the Global Frontier Hybrid Interface Materials (GFHIM) of the National Research Foundation (NRF) of Korea funded by the Ministry of Science, ICT & Future Planning (2013M3A6B1078870). J.R.M., V.R.C., and the initial work of Y.I. were supported from the U.S. Department of

Energy, Office of Science, Basic Energy Sciences, Materials Sciences and Engineering Division. The Monte Carlo simulation work performed by L.V. was supported by the U.S. Department of Energy, Office of Science, Basic Energy Sciences, Chemical Sciences, Geosciences, and Biosciences Division. This research used resources of the National Energy Research Scientific Computing Center, which is supported by the Office of Science of the U.S. Department of Energy under Contract No. DEAC02-05CH11231. P.C. was supported by DOE grant No. DE-FG02-08ER46491 and T.T. acknowledges support from NSF grant No. DMR-1145968. In addition, T.T. acknowledges generous support from the Simons Foundation through Grant No. 391888, which endowed his sabbatical at MIT. T.T. and P.C. acknowledges early calculations by Daniel Johnson at WFU.

■ REFERENCES

- (1) Lin, L. C.; Berger, A. H.; Martin, R. L.; Kim, J.; Swisher, J. A.; Jariwala, K.; Rycroft, C. H.; Bhowan, A. S.; Deem, M. W.; Haranczyk, M.; et al. In Silico Screening of Carbon-Capture Materials. *Nat. Mater.* **2012**, *11*, 633–641.
- (2) Wilmer, C. E.; Snurr, R. Q. Large-Scale Generation and Screening of Hypothetical Metal-Organic Frameworks for Applications in Gas Storage and Separations. *Top. Curr. Chem.* **2013**, *345*, 257–289.
- (3) Colon, Y. J.; Snurr, R. Q. High-Throughput Computational Screening of Metal-Organic Frameworks. *Chem. Soc. Rev.* **2014**, *43*, 5735–5749.
- (4) Furukawa, H.; Cordova, K. E.; O’Keeffe, M.; Yaghi, O. M. The Chemistry and Applications of Metal-Organic Frameworks. *Science* **2013**, *341*, 1230444.
- (5) Liu, J.; Lee, J. Y.; Pan, L.; Obermyer, R. T.; Simizu, S.; Zande, B.; Li, J.; Sankar, S. G.; Johnson, J. K. Adsorption and Diffusion of Hydrogen in a New Metal-Organic Framework Material: [Zn(Bdc)-(Ted)(0.5)]. *J. Phys. Chem. C* **2008**, *112*, 2911–2917.
- (6) Hulvey, Z.; Vlasisavljevich, B.; Mason, J. A.; Tsivion, E.; Dougherty, T. P.; Bloch, E. D.; Head-Gordon, M.; Smit, B.; Long, J. R.; Brown, C. M. Critical Factors Driving the High Volumetric Uptake of Methane in Cu-3(Btc)(2). *J. Am. Chem. Soc.* **2015**, *137*, 10816–10825.
- (7) Ihm, Y.; Cooper, V. R.; Peng, L. J.; Morris, J. R. The Influence of Dispersion Interactions on the Hydrogen Adsorption Properties of Expanded Graphite. *J. Phys.: Condens. Matter* **2012**, *24*, 424205.
- (8) Ihm, Y.; Cooper, V. R.; Gallego, N. C.; Contescu, C. I.; Morris, J. R. Microstructure-Dependent Gas Adsorption: Accurate Predictions of Methane Uptake in Nanoporous Carbons. *J. Chem. Theory Comput.* **2014**, *10*, 1–4.
- (9) Peng, L. J.; Morris, J. R. Prediction of Hydrogen Adsorption Properties in Expanded Graphite Model and in Nanoporous Carbon. *J. Phys. Chem. C* **2010**, *114*, 15522–15529.
- (10) Peng, L. J.; Morris, J. R. Structure and Hydrogen Adsorption Properties of Low Density Nanoporous Carbons from Simulations. *Carbon* **2012**, *50*, 1394–1406.
- (11) Morris, J. R.; Contescu, C. I.; Chisholm, M. F.; Cooper, V. R.; Guo, J.; He, L.; Ihm, Y.; Mamontov, E.; Melnichenko, Y. B.; Olsen, R. J.; et al. Modern Approaches to Studying Gas Adsorption in Nanoporous Carbons. *J. Mater. Chem. A* **2013**, *1*, 9341–9350.
- (12) Lee, J. Y.; Olson, D. H.; Pan, L.; Emge, T. J.; Li, J. Microporous Metal-Organic Frameworks with High Gas Sorption and Separation Capacity. *Adv. Funct. Mater.* **2007**, *17*, 1255–1262.
- (13) Linstrom, P. J.; Mallard, W. G. The NIST Chemistry Webbook: A Chemical Data Resource on the Internet. *J. Chem. Eng. Data* **2001**, *46*, 1059–1063.
- (14) Leachman, J. W.; Jacobsen, R. T.; Penoncello, S. G.; Lemmon, E. W. Fundamental Equations of State for Parahydrogen, Normal Hydrogen, and Orthohydrogen. *J. Phys. Chem. Ref. Data* **2009**, *38*, 721.
- (15) Hansen, J.; McDonald, I. R. *Theory of Simple Liquids with Applications to Soft Matter*; Academic Press: Oxford, UK, 2013.

(16) Wu, H.; Zhou, W.; Yildirim, T. High-Capacity Methane Storage in Metal-Organic Frameworks M-2(Dhtp): The Important Role of Open Metal Sites. *J. Am. Chem. Soc.* **2009**, *131*, 4995–5000.

(17) Dion, M.; Rydberg, H.; Schroder, E.; Langreth, D. C.; Lundqvist, B. I. Van Der Waals Density Functional for General Geometries. *Phys. Rev. Lett.* **2004**, *92*, 246401.

(18) Giannozzi, P.; Baroni, S.; Bonini, N.; Calandra, M.; Car, R.; Cavazzoni, C.; Ceresoli, D.; Chiarotti, G. L.; Cococcioni, M.; Dabo, I. Quantum Espresso: A Modular and Open-Source Software Project for Quantum Simulations of Materials. *J. Phys.: Condens. Matter* **2009**, *21*, 395502.

(19) Thonhauser, T.; Cooper, V. R.; Li, S.; Puzder, A.; Hyldgaard, P.; Langreth, D. C. Van Der Waals Density Functional: Self-Consistent Potential and the Nature of the Van Der Waals Bond. *Phys. Rev. B: Condens. Matter Mater. Phys.* **2007**, *76*, 125112.

(20) Cooper, V. R. Van Der Waals Density Functional: An Appropriate Exchange Functional. *Phys. Rev. B: Condens. Matter Mater. Phys.* **2010**, *81*, 161104.

(21) Berland, K.; Cooper, V. R.; Lee, K.; Schroder, E.; Thonhauser, T.; Hyldgaard, P.; Lundqvist, B. I. Van Der Waals Forces in Density Functional Theory: A Review of the Vdw-Df Method. *Rep. Prog. Phys.* **2015**, *78*, 066501.

(22) Buch, V. Path Integral Simulations of Mixed Para-D2 and Ortho-D2 Clusters: The Orientational Effects. *J. Chem. Phys.* **1994**, *100*, 7610.

(23) Rappe, A. K.; Casewit, C. J.; Colwell, K. S.; Goddard, W. A., III; Skiff, W. M. Uff, a Full Periodic Table Force Field for Molecular Mechanis and Molecular Dynamics Simulations. *J. Am. Chem. Soc.* **1992**, *114*, 10024–35.

(24) Rodriguez-Cantano, R.; de Tudela, R. P.; Bartolomei, M.; Hernandez, M. I.; Campos-Martinez, J.; Gonzalez-Lezana, T.; Villarreal, P.; Hernandez-Rojas, J.; Breton, J. Examination of the Feynman-Hibbs Approach in the Study of Ne-N-Coronene Clusters at Low Temperatures. *J. Phys. Chem. A* **2016**, *120*, 5370–5379.

(25) Celli, M.; Bafle, U.; Cuello, G. J.; Formisano, F.; Guarini, E.; Magli, R.; Neumann, M.; Zoppi, M. Microscopic Structure Factor of Liquid Hydrogen by Neutron-Diffraction Measurements. *Phys. Rev. B: Condens. Matter Mater. Phys.* **2005**, *71*, 014205.

(26) Dietzel, P. D. C.; Besikiotis, V.; Blom, R. Application of Metal-Organic Frameworks with Coordinatively Unsaturated Metal Sites in Storage and Separation of Methane and Carbon Dioxide. *J. Mater. Chem.* **2009**, *19*, 7362–7370.

(27) Kong, L. Z.; Cooper, V. R.; Nijem, N.; Li, K. H.; Li, J.; Chabal, Y. J.; Langreth, D. C. Theoretical and Experimental Analysis of H-2 Binding in a Prototypical Metal-Organic Framework Material. *Phys. Rev. B: Condens. Matter Mater. Phys.* **2009**, *79*, 081407.

(28) Cooper, V. R.; Kong, L.; Langreth, D. C. Computing Dispersion Interactions in Density Functional Theory. *Phys. Procedia* **2010**, *3*, 1417–1430.

(29) Garberoglio, G.; Skoulidas, A. I.; Johnson, J. K. Adsorption of Gases in Metal Organic Materials: Comparison of Simulations and Experiments. *J. Phys. Chem. B* **2005**, *109*, 13094–13103.

(30) Canepa, P.; Nijem, N.; Chabal, Y. J.; Thonhauser, T. Diffusion of Small Molecules in Metal Organic Framework Materials. *Phys. Rev. Lett.* **2013**, *110*, 026102.

(31) Canepa, P.; Arter, C. A.; Conwill, E. M.; Johnson, D. H.; Shoemaker, B. A.; Soliman, K. Z.; Thonhauser, T. High-Throughput Screening of Small-Molecule Adsorption in Mof. *J. Mater. Chem. A* **2013**, *1*, 13597–13604.